Structural and optical properties of dilute InAsN grown by molecular beam epitaxy

J. Ibáñez,[1,a)] R. Oliva,[1] M. De la Mare,[2] M. Schmidbauer,[3] S. Hernández,[4] P. Pellegrino,[4] D. J. Scurr,[5] R. Cuscó,[6] L. Artús,[6] M. Shafi,[6] R. H. Mari,[6] M. Henini,[6] Q. Zhuang,[2] A. Godenir,[2] and A. Krier[2]

[1]*Institut Jaume Almera, Consell Superior d'Investigacions Científiques (CSIC), Lluís Solé i Sabarís s.n, 08028 Barcelona, Catalonia, Spain*
[2]*Department of Physics, Lancaster University, Lancaster LA1 4YB, United Kingdom*
[3]*Leibniz Institute for Crystal Growth, Max-Born-Str. 2, D-12489 Berlin, Germany*
[4]*Department of Electronics, MIND-IN2UB, University of Barcelona, Martí i Franqués 1, 08028 Barcelona, Catalonia, Spain*
[5]*School of Pharmacy, University of Nottingham, Nottingham NG7 2RD, United Kingdom*
[6]*School of Physics and Astronomy, University of Nottingham, Nottingham NG7 2RD, United Kingdom*

(Received 23 September 2010; accepted 30 September 2010; published online 17 November 2010)

We perform a structural and optical characterization of $InAs_{1-x}N_x$ epilayers grown by molecular beam epitaxy on InAs substrates ($x \lesssim 2.2\%$). High-resolution x-ray diffraction (HRXRD) is used to obtain information about the crystal quality and the strain state of the samples and to determine the N content of the films. The composition of two of the samples investigated is also obtained with time-of-flight secondary ion mass spectroscopy (ToF-SIMS) measurements. The combined analysis of the HRXRD and ToF-SIMS data suggests that the lattice parameter of InAsN might significantly deviate from Vegard's law. Raman scattering and far-infrared reflectivity measurements have been carried out to investigate the incorporation of N into the InAsN alloy. N-related local vibrational modes are detected in the samples with higher N content. The origin of the observed features is discussed. We study the compositional dependence of the room-temperature band gap energy of the InAsN alloy. For this purpose, photoluminescence and optical absorption measurements are presented. The results are analyzed in terms of the band-anticrossing (BAC) model. We find that the room-temperature coupling parameter for InAsN within the BAC model is $C_{NM}=2.0\pm0.1$ eV.
 [doi:10.1063/1.3509149]

I. INTRODUCTION

Dilute III-V nitride semiconductors have attracted considerable attention in recent years owing to their unusual optical and electronic properties (i.e., strong band gap reduction and bowing with increasing N content, large nonparabolicity of the conduction band, anomalous dependence of the electron effective mass on N composition, strong carrier localization effects, etc.).[1] Such remarkable fundamental properties could be exploited to develop novel device applications for optoelectronics, terahertz electronics and solar cell technology. In particular, due to its narrow band gap, dilute $InAs_{1-x}N_x$ is a very promising candidate for the design and fabrication of optoelectronic devices operating in the midinfrared spectral region (3–5 μm).[2]

InAsN epilayers have been grown on different substrates such as GaAs (Refs. 3–7), InP (Refs. 8–10), and InAs (Refs. 11–13). Also, highly strained laser structures based on InAsN/InGaAs quantum wells grown on InP have been reported.[14] However, in spite of the strong interest of InAsN both from fundamental and applied points of view, relatively little is known about this dilute nitride semiconductor in comparison to Ga(In)AsN alloys, which have been the subject of intense research effort in the last decade.[1]

It is well known that the structural and optical quality of dilute nitrides rapidly degrades with increasing N content. In the case of InAsN, it is in general difficult to produce high-quality material with appreciable levels of activated nitrogen. Previous investigations concluded that the amount of N incorporated into InAs is systematically lower than that measured in GaAs.[15] Strong deviations from Vegard's law have been observed in the N-content dependence of the lattice parameter of highly mismatched alloys like GaAsN.[16] In the case of InAsN, first principles calculations predict that Vegard's law is not valid even for very dilute N concentrations.[17] N-related local vibrational modes (LVMs) have been observed by Raman scattering in InAsN samples.[10] The observed LVMs were tentatively assigned to N_{As} and to N–In–N complexes. Other N configurations involving nonsubstitutional N could yield important distortions of the lattice (i.e., strong deviations of Vegard's law).

Regarding the optical properties of InAsN, Veal *et al.*[11] reported weak 3.5 μm photoluminescence (PL) emission at 77 K in $InAs_{1-x}N_x$/InAs epilayers with a N content of N $=2.2\%$. In that work, a severe degradation of the PL emission was observed with increasing N content. More recently, the effect of the growth conditions on the incorporation of N in InAsN/InAs epilayers was investigated.[12,13] High quality samples with nitrogen compositions up to 2.5% were obtained, with intense low-temperature PL emission and relatively strong room-temperature (RT) PL emission at a wave-

[a)]Electronic mail: jibanez@ictja.csic.es.

length of 4.5 μm. Photoreflectance (PR) studies on similar epilayers allowed probing the dependence on N content of both the band gap and the spin-orbit splitting of InAsN up to a N concentration of 0.88%.[18] It was concluded that only the conduction states are affected by N, in agreement with the results obtained in the Ga(In)AsN alloy system and fully consistent within the framework of the band-anticrossing (BAC) model.[19]

In the present work we use a series of structural and optical characterization techniques to study $InAs_{1-x}N_x$ epilayers grown by molecular beam epitaxy (MBE) on InAs substrates. Samples with N contents ranging from 0% to 2.2% are investigated. High-resolution x-ray diffraction (HRXRD) is used to evaluate the N composition of the films. Information about the crystal quality and the strain state of the samples as a function of N content is obtained. We perform time-of-flight secondary ion mass spectroscopy (ToF-SIMS) in two of the samples investigated, one with low N content and one with high N content. We find that the N content obtained by ToF-SIMS in the N-rich sample is higher than that derived from the HRXRD measurements. Since Vegard's law was assumed to evaluate the N content from the HRXRD reflections, this suggests that the lattice parameter of InAsN might significantly deviate from Vegard's law owing to the incorporation of nonsubstitutional N in the lattice. Raman scattering measurements were carried out in order to characterize the crystal quality of the samples and obtain information about the nitrogen incorporation. N-related LVMs are detected in the samples with higher N content. The origin of the observed Raman features is discussed and far-infrared (FIR) reflectivity measurements on InAsN/GaAs are also performed to support the assignments of the Raman bands. PL and optical transmission measurements are presented, and the dependence on N composition of the band gap energy for the InAsN alloy is obtained. The results are analyzed in terms of the BAC model and the different mechanisms involved in the optical emission and absorption experiments in the InAsN alloy are discussed.

II. EXPERIMENT

$InAs_{1-x}N_x$ epilayers with N contents up to $N \lesssim 2.2\%$ were grown at 400 °C by plasma-assisted MBE on epiready (100)-oriented n^+-InAs substrates. The nominal growth rate was 0.9 μm/h, and the nominal epilayer thickness was ~ 1 μm. The samples were nominally undoped, but Hall effect measurements revealed a background electron concentration of $\sim 10^{17}$ cm^{-3}.

HRXRD measurements were carried out with a double-crystal diffractometer, equipped with a parabolic (focusing) multilayer mirror and a four-bounce Ge 220 Bartels monochromator (Cu $K_{\alpha 1}$ line, $\lambda = 1.5406$ Å). The angular resolution in the scattering plane was $\Delta\theta = 11$ arcsec. Table I contains information about the N composition of the films and their degree of plastic relaxation as obtained from the HRXRD measurements (see discussion below).

A ToF-SIMS IV (IONTOF Gmbh, Münster, Germany) time-of-flight secondary ion mass spectrometer was used to perform the depth profiles. The instrument was equipped with both a 5 keV Cs^+ ion source and a 25 keV cluster Bi^+ ion source, which were, respectively, employed for sputtering and analysis, both set at incident angles of 45°. In order to avoid any problems occurring due to overlap of the analyzed area with regions that have not received a constant Cs^+ ion dose, the Cs^+ sputter area was set to 300×300 μm^2 area and only the central 100×100 μm^2 area was analyzed with the Bi_3^+ ion beam.

TABLE I. Molar fraction of N (N_{XRD}) and plastic relaxation (R) of the InAsN/InAs epilayers studied in this work, as obtained by HRXRD. Samples A0174 and A0146 exhibit two dominant N compositions inside the layer. The N_{XRD} values in parentheses indicate the composition of the second dominant domain. Sample A0200 contains both coherent and relaxed areas with different R values.

Sample	N content (N_{XRD}) (%)	Plastic relaxation (R)
A0174	0.34(0.55)	<0.01
A0146	0.62(0.75)	<0.01
A0142	0.83	<0.01
A0206	1.2	<0.01
A0200	1.4(1.3)	<0.01, 0.23
A0203	1.5	0.31
A0208	2.2	0.08

The pulsed Bi_3^+ analysis beam had a spot size of <2 μm diameter and was rastered in a 256×256 pixel array. Owing to the materials conductivity, charge compensation using an electron flood gun was not required. The sputtering and analysis ion beams were aligned before measurements so that the spectral analysis area was at the center of the sputter crater.

RT PL measurements were excited with the 514.5 nm line of an Ar^+ laser. We used output powers of the laser of up to 1.6 W, with a spot diameter on the sample of ~ 1 mm. The PL measurements were recorded with a IFS 66/S Fourier-transform IR (FTIR) spectrometer and an InSb photodiode detector cooled at 77 K and connected to a lock-in amplifier. The temperature and power dependence of the PL emission of these samples was the subject of previous work.[12,13]

Optical absorption experiments were recorded by using a BOMEM DA.8 rapid scanning FTIR interferometer. For these measurements, a globar source, a KBr beam-splitter and an MCT detector were employed. RT unpolarized infrared reflectivity experiments were also carried out with this FTIR system. In this case, detection was done by using a deuterated triglycine sulfate (DTGS) detector. The optical absorption (reflectivity) measurements were typically recorded with 4 cm^{-1} (2 cm^{-1}) resolution and 100 coadditions. In the reflectivity configuration, the angle between the incident and reflected beams and the normal to the sample surface was $\sim 45°$.

Raman scattering measurements were acquired at RT and at 80 K by using the double subtractive configuration of a Jobin-Yvon T64000 spectrometer equipped with a liquid N_2-cooled charged coupled device. The 488.0 and the 514.5 nm lines of an Ar^+ laser were used as excitation source. All

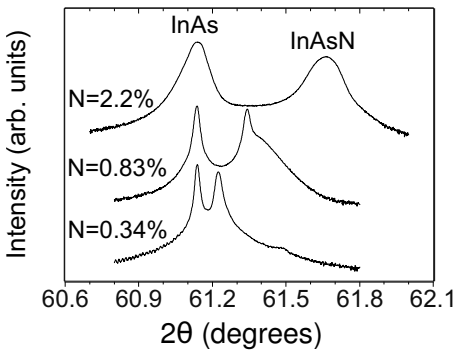

FIG. 1. HRXRD rocking curves of three different InAsN epilayers grown by MBE on InAs substrates. The curves have been vertically shifted for convenience. Note that a logarithmic intensity scale has been used.

the experiments were performed in a $x'(y'y')\bar{x}'$ backscattering configuration [$x'=(110)$ and $y'=(1\bar{1}0)$], with 100 μm slits.

III. RESULTS AND DISCUSSION

A. HRXRD characterization

HRXRD measurements were performed in order to obtain information about the N content, the crystal quality, the strain state, and the thickness of the InAsN films. Figure 1 shows selected x-ray rocking curves [symmetrical (004) reflections] of the samples studied in this work. Reflections from both the InAs substrate and the InAsN epilayers are observed. As expected, the Bragg angle corresponding to the $InAs_{1-x}N_x$ reflection increases with increasing N content. In the case of the sample with $N_{XRD}=0.83\%$ as obtained from the analysis of the HRXRD (see discussion below), a tail on the large angle side of the InAsN reflection is observed, indicating that there is a vertical N composition gradient in this layer.

Reciprocal space maps [asymmetrical (224) reflections] were obtained for all the samples. Results for two of the samples are shown in Figs. 2(a) and 2(b) (samples with $N_{XRD}=0.62$ and 1.5%). Two different layer peaks, which overlap and give rise to an elongated spot, appear in the vertical wave vector ($q_\perp$) direction of the map in the case of the sample with $N_{XRD}=0.62\%$ [Fig. 2(a)]. This was also observed in the samples with $N_{XRD}=0.34\%$ and $N_{XRD}=1.4\%$ (not shown) and suggests that there exist two dominant N compositions within these layers.

The determination by HRXRD of the composition of ternary alloys is a standard procedure that relies on Vegard's law for the lattice parameter (a) of the alloy. From the asymmetrical reflections, both the vertical and horizontal lattice deformations of the epilayer relative to the substrate, $(\Delta d/d)_\perp$ and $(\Delta d/d)_\parallel$, are obtained (d is the interplanar spacing). With these values, the relaxed lattice mismatch between the InAsN epilayer and the InAs substrate ($\Delta a/a$) is determined, and the concentration of substitutional N in the films (N_{XRD}) is then evaluated by assuming Vegard's law for the lattice parameter of $InAs_{1-x}N_x$. The second column of Table I displays the resulting N_{XRD} values for the samples studied in this work. Possible sources of error arise from the uncertainty in Vegard's law and also from the presence of vertical N composition gradients and/or the presence of domains with different N contents.

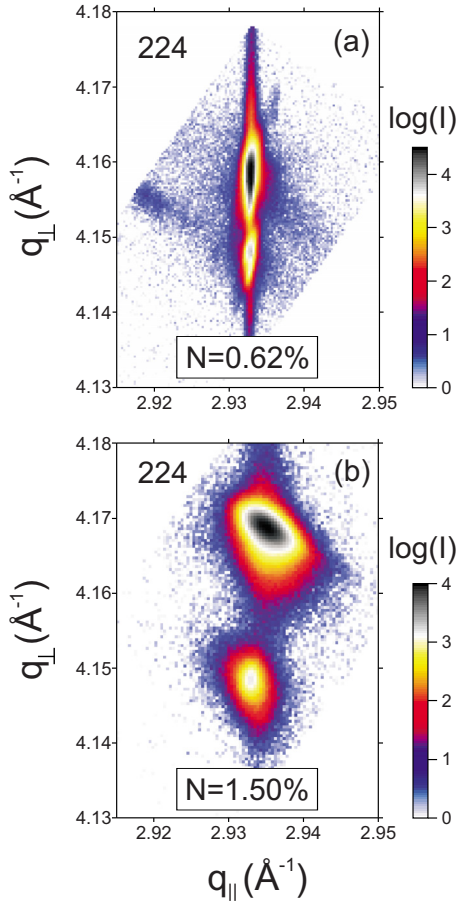

FIG. 2. (Color online) X-ray reciprocal space maps of two InAsN/InAs epilayers with (a) $N_{XRD}=0.62\%$ and (b) $N_{XRD}=1.5\%$ in the vicinity of the 224 InAs reciprocal lattice point.

The third column of Table I shows the degree of plastic relaxation, $R=(\Delta d/d)_\parallel/(\Delta a/a)$. We find that the InAsN layers with lowest N contents ($N_{XRD}\leq 1.2\%$) are pseudomorphically grown on the InAs substrate, since $R\sim 0$. The Bragg reflections for these samples in the reciprocal maps are narrow in the horizontal wave vector direction ($q_\parallel$) and appear at identical $q_\parallel$ values [see Fig. 2(a)]. These samples exhibit considerable x-ray diffuse scattering, most likely caused by misfit dislocations and other defects within the InAsN layer.

In the case of the samples with higher N contents ($N_{XRD}=1.4$, 1.5, and 2.2%), both the symmetric and asymmetric Bragg reflections turn out to be fairly broad, indicating a larger defect density in comparison to the samples with lower N concentrations (i.e., a larger amount of misfit dislocations). This is illustrated in Fig. 2(b) for the sample with $N_{XRD}=1.5\%$. In the particular case of the sample with $N_{XRD}=1.4\%$ (not shown), the reciprocal space map indicates that this epilayer contains both coherent and relaxed areas. This result suggests that plastic relaxation starts around this N composition value in these samples.

In the case of the sample with $N_{XRD}=0.34\%$, the rocking curves display thickness fringes (see Fig. 1). From the angular distance between the fringes, we estimate that the thick-

ness of this epilayer is around 780 nm. Thickness fringes were also observed in the sample with an N composition of 1.2% (not shown). We obtain a thickness of ~300 nm for this film. Given that the nominal thickness of these epilayers is 1000 nm, the thickness values determined from the analysis of the fringes may suggest that the growth rate decreases with increasing N concentration. The fact that thickness fringes are observed in these two samples is a consequence of a good interface quality resulting from the coherent (pseudomorphic) growth. In the case of the samples with N_{XRD}=0.62 and 0.83%, also coherently grown on the InAs substrate as revealed by the reciprocal space mapings, the rocking curves do not show thickness fringes, which may be attributed to an inhomogeneous strain distribution in the epilayer and a poorer interface quality.

B. ToF-SIMS

ToF-SIMS measurements were performed in two of the samples investigated in this work, namely, the sample with the lowest N content (N_{XRD}=0.34%) and that with the highest N content (N_{XRD}=2.2%). The aim of the ToF-SIMS study was twofold: first, to investigate the unintentional incorporation of impurities in the samples. Second, to determine the total amount of N incorporated into the InAsN epilayers and compare the resulting value with the HRXRD data.

Residual impurities like C, O, or H are typical of MBE growth. For instance, carbon contamination may arise from hot elements (i.e., filaments) yielding strong outgassing. Also, the Knudsen cells may contribute due to the presence of contaminants in the pyrolitic boron nitride crucibles or even in the evaporated materials. In the case of our InAsN samples, the ToF-SIMS analysis did not reveal the presence of any sizeable amount of unintentional impurities in the two samples investigated, which confirms that the as-grown material is of high purity. This result is relevant for the interpretation of the Raman experiments (see below), since we can rule out that any of the LVMs observed in these samples arise from contaminants.

To evaluate the total N content of the two samples investigated, we used the average intensity of a secondary ion peak that was assigned to $CsAsN^+$ adducts. It should be noted that the only indication of the N content that we were able to find in the positive spectra arises from this signal. While similar levels of As^+ were found in the two samples investigated and also in InAs blank material, clear differences in the $CsAsN^+$ peak were found between the two InAsN samples (and no $CsAsN^+$ signal was found in the blank material). This, together with the fact that the assignment of the $CsAsN^+$ peak had an accuracy of <50 ppm, confirms the validity of this peak to evaluate the N content of the InAsN epilayers.

Although the Tof-SIMS technique is not inherently quantitative, comparisons between spectra of similar materials can still be made in order to evaluate their composition. The difference in the average $CsAsN^+$ secondary ion yield between the two InAsN samples indicated that the N content of the N-rich sample is ~6.8 times larger than that of the sample with the lowest N content. Thus, by assuming that the N content obtained by HRXRD and ToF-SIMS in the N-poor sample is nearly the same (0.34%), we conclude that the total N content of the N-rich sample is around 5% larger than the value obtained by HRXRD. Note that this value would have been even larger if we had considered larger N_{XRD} values from regions of this sample with higher N contents (N_{XRD} =0.55%, see Table I). Similar results are found in dilute $GaAs_{1-x}N_x$,[16] where deviations of Vegard's law were observed for $x \gtrsim 2\%-3\%$. Such deviations were accounted for by nonsubstitutional N configurations within the highly mismatched alloy. In the case of the present study, taking into account the errors associated with the HRXRD and ToF-SIMS techniques, no definitive conclusions can be drawn. However, the combined analysis of the HRXRD and ToF-SIMS data points in the direction that an important amount of nonsubstitutional N is incorporated into InAsN, casting some doubt on the validity of Vegard's law to describe the lattice parameter of the InAsN alloy even for N contents as low as 2%–3%. Further investigations dealing with samples with higher N contents would be desirable in order to fully ascertain the amount of nonsubstitutional N that is incorporated into the dilute InAsN alloy.

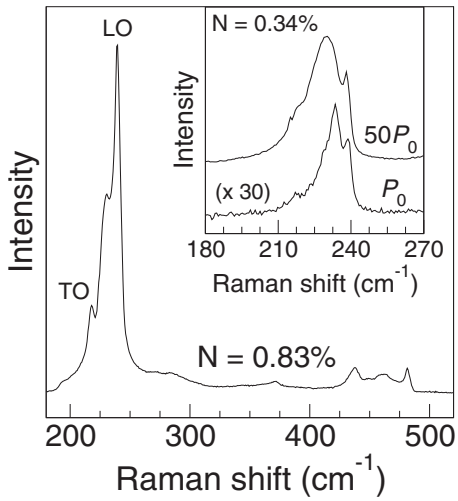

FIG. 3. Low-temperature (80 K) macro-Raman spectrum of an InAsN/InAs epilayer with N_{XRD}=0.83%. Inset: first-order Raman spectra at 300 K of an InAsN/InAs epilayer with N_{XRD}=0.34%. These spectra were performed with a micro-Raman setup (×100 objective). The lower spectrum was excited with a reduced laser power (P_0), yielding a power density on the sample lower than 10^5 W cm^{-2}. The upper curve was excited with a laser power of ~$50P_0$.

C. Vibrational spectroscopies

Raman spectroscopy is a standard technique for the study of the lattice dynamics, the crystal quality, the composition and the strain state of semiconductor materials and structures. Raman scattering by LVMs allows one to obtain relevant information about the local bonding of impurities, as for instance N into dilute nitrides. In the present work, we use Raman scattering to characterize our InAsN samples and to study the incorporation of N into the lattice.

Figure 3 shows a typical Raman spectrum, acquired at 80 K, of the InAsN alloy (N_{XRD}=0.83%). The spectra are dominated by the InAs-like longitudinal optical (LO) mode,

located at around 240 cm^{-1}. The fact that this peak only suffers a minor broadening relative to undoped InAs shows that the crystallinity of this sample is not affected substantially by the incorporation of N. Two features are observed in the low-frequency side of the LO mode: first, a weak peak at around 215 cm^{-1}, which corresponds to the forbidden InAs-like transverse optical (TO) mode. This peak is observed due to a disorder-induced relaxation of the selection rules, as occurs for instance in dilute GaAsN.[20] In the particular case of the spectrum displayed in Fig. 3, both the InAs-like TO and LO modes are slightly shifted to lower frequencies with respect to bulk InAs (we measure TO and LO frequencies at 80 K for bulk InAs grown on GaAs at 220 cm^{-1} and 242 cm^{-1}, respectively; Carles *et al.*[21] report similar values). These frequency shifts, also observed in the case of the GaAs-like LO and TO modes of GaAsN (Refs. 22 and 20) and in the GaAs- and InAs-like LO modes of InGaAsN,[23] reflect the strain state of the epilayers as well as the effect of alloying on the phonon frequencies.[20]

A clear feature is observed between the InAs-like TO and LO peaks. A similar Raman band has been previously observed in *n*-type InAs samples and attributed to an LO-plasmon coupled mode (LOPCM).[24] To further investigate the origin of this feature in the case of the undoped InAsN epilayers, we show in the inset of Fig. 3 Raman spectra of the InAsN sample with the lowest N content (0.34%). Both spectra were acquired with a micro-Raman setup in order to obtain high power density excitation conditions (×100 objective). The lower spectrum in the inset was excited with a reduced laser power, yielding power densities on the sample lower than 10^5 W cm^{-2}. The upper curve was obtained with a power density around 50 times larger. As can be seen in the inset of Fig. 3, under a high power density the LO mode is slightly downshifted relative to the low excitation conditions. This frequency shift can be attributed to sample heating. Interestingly, the band located between the TO and LO peaks suffers a clear broadening and frequency downshift. This behavior is the same as displayed by the low-frequency LOPCM that appears in the Raman spectra of *n*-type InAs.[24] The fact that this low-frequency LOPCM in *n*-type material lies between the TO and LO modes is usually attributed to large-wave vector scattering arising from disorder or absorption effects (see Ref. 24 and references therein). Alternatively, a more simple approach dealing with overdamped LOPCMs, (i.e., LOPCMs with lifetimes much shorter than the oscillation period of the collective excitation) is also able to account for the behavior of the LOPCM in InAs. This approach has been successfully used to describe the LO-plasmon coupling in *p*-type GaAs (Ref. 25) or in *n*-type dilute GaAsN.[26]

Leaving aside the actual mechanism responsible for the behavior of the LOPCMs in InAs, here, we tentatively assign the feature that appears in the Raman spectra of InAsN between the TO and LO modes to a short-lived photoexcited LOPCM, arising from the coupling between the LO mode and the free carriers photogenerated by the excitation radiation. It should be emphasized that this feature was observed both in undoped InAs samples and in N-rich InAsN epilayers. However, we were not able to find any clear correlation between the degree of photoexcitation and the N content of the epilayers. Thus, it cannot be ruled out that disorder, which could be related to N doping and which could be enhanced by laser-induced damage, may originate the observed Raman signal in this frequency region. Note that no L^+ modes were detected in any of the samples. This is in contrast to what occurs in *n*-InAs.[24] In the case of photoexcited LOPCMs, however, the absence of L^+ bands may be attributed to a lower lifetime of the photoexcited LOPCMs in comparison to those occurring in *n*-type InAs. Also, the inhomogeneous distribution of the photogenerated-free carriers may hinder the appearance of the L^+ modes in the Raman spectra (for a detailed discussion of these topics, see for instance Refs. 27 and 28). More work is required in order to confirm that the observed feature arises from photoexcitation effects. Clearly, the study of the photoexcited LOPCMs in InAs and InAsN and, in particular, the role of N on the power density dependence of the LOPCMs in this compound is beyond the scope of this work.

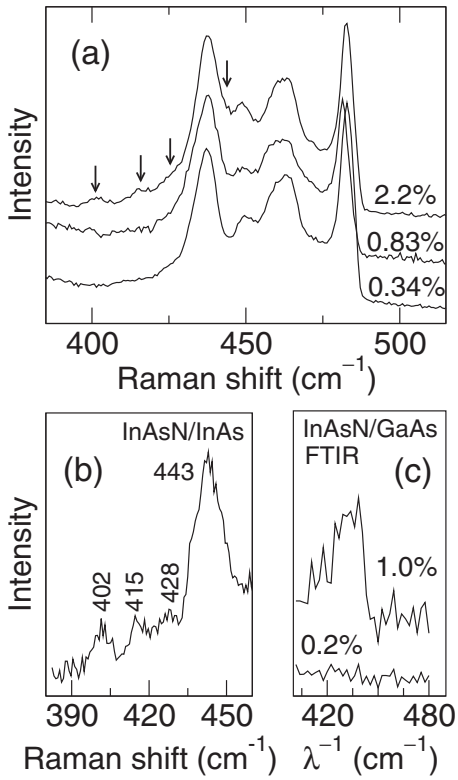

FIG. 4. (a) Detailed Raman spectra, acquired at 80 K, showing the second-order optical peaks of three different InAsN/InAs epilayers with N_{XRD} =0.34%, 0.83%, and 2.2%. The arrows indicate the presence of weak N-related features in the Raman spectrum of the sample with N_{XRD}=2.2%. (b) Difference spectrum obtained after subtracting the Raman spectra of the sample containing the highest (2.2%) and lowest (0.34%) N contents. (c) FTIR reflectivity spectrum of two different InAsN epilayers grown on GaAs substrates.

Figure 4(a) shows Raman spectra of three different InAsN epilayers in the 400–500 cm^{-1} range. Besides the second-order optical modes of InAs, located at ~435, 450, 460, and 480 cm^{-1},[21] four very weak features show up in the spectra of the sample with the highest N content (upper curve, N_{XRD}=2.2%). Such features, marked with an arrow in Fig. 4(a), are centered at 402, 415, 428, and 443 cm^{-1}. Note

that the feature at 443 cm^{-1} is only apparent as a slight broadening of the high-frequency tail of the 2TO mode, located at 435 cm^{-1}. In order to better discern these features, we show in Fig. 4(b) the difference between the spectra of the sample containing the highest and lowest N contents (2.2% and 0.34%, respectively). All four peaks are clearly seen in the difference spectrum. The modes at 402, 415, and 443 cm^{-1} were previously reported by Wagner *et al.*[10] in Raman difference spectra of dilute InAsN epilayers with N =1.2%.

With regard to the stronger band, centered at 443 cm^{-1}, it has previously been assigned to isolated N_{As} LVM.[10,29] However, there is some ambiguity in the assignment of this band because it is usually revealed in difference spectra, and there are strong second-order optical modes from the InAs matrix in this frequency range. In order to confirm the origin of this feature, we performed FIR reflectivity measurements on InAsN/GaAs epilayers grown by MBE. Details of the samples used for these experiments are described elsewhere.[7] It should be emphasized that in Raman scattering measurements on highly-absorbing InAsN the weak Raman signal of the N-related LVMs cannot be discriminated from the second-order modes arising from the InAs matrix. In the case of FIR measurements on InAsN/InAs epilayers, the extremely weak absorption arising from the second-order optical modes of InAs may yield relatively deep transmission dips owing to the large volume of the InAs substrate in relation to the InAsN epilayer. This problem is overcome with FIR measurements on InAsN/GaAs samples, since the response from the second-order modes within the InAsN thin film is negligible. We show in Fig. 4(c) FIR reflectivity spectra from two different InAsN/GaAs samples with nominal N compositions of 0.2% and 1%. It can be seen that the feature at 443 cm^{-1} is only visible in the spectrum of the sample with higher N content. A very weak feature was also observed in a sample with a N content of 0.6% (not shown). These observations confirm that the band at 443 cm^{-1}, detected by Raman scattering, is not a spurious effect arising from the subtraction of Raman spectra. Taking into account that this band is the most prominent among the LVM peaks detected by Raman scattering [see Fig. 4(b) and also Ref. 10], this result confirms that the band at 443 cm^{-1} is originated by substitutional $^{14}N_{As}$.

With regard to the weak Raman features between 400 and 430 cm^{-1}, it should first be mentioned that weak bands are observed in the Raman spectra of bulk InAs at ~405 and 425 cm^{-1}.[21] Note also that a faint, broad structure is visible around 425 cm^{-1} in the case of the sample with N_{XRD} =0.34% [lower curve of Fig. 4(a)]. We assign this band to a second-order mode from the InAs matrix. The feature at 402 cm^{-1} is not observed in the N-poor sample [Figs. 4(a) and 4(b)], and this confirms that it is N-related. The same argument holds for the feature at 415 cm^{-1}.

Different N configurations may be involved in these two LVMs at 402 and 415 cm^{-1}. Wagner *et al.*[10] tentatively assigned these peaks to In-N complexes of higher order involving nearest neighbor N–In–N vibrations (i.e., InN_2As_2 complexes and higher orders). However, it should be noted that in the dilute alloy (N contents below 3%) the randomly distributed N atoms are located far away from each other within the crystal lattice (see discussion in Ref. 30 for the case of dilute GaAsN). Thus, only a single N_{As} LVM peak is detected by Raman scattering in high-quality GaAsN samples up to a N content of 3%.[22] In addition, the influence of second-nearest neighbor N–N pairs on the frequency of the isolated N substitutional is expected to be very small.[30] Thus, we speculate that the peaks at 402 and 415 cm^{-1} do not arise from N–In–N complexes but from other N-related nonsubstitutional configurations like N–N or N–As split interstitials or even from N antisites or interstitial N. With regard to this, density-functional theory calculations in dilute GaAsN predict a LVM associated to N–N split interstitials located at 419 cm^{-1}, below the isolated substitutional LVM.[30] However, these same calculations predict that As–N split interstitials lie well above the isolated N substitutional LVM in GaAsN.[30] Theoretical work dealing with the N-related LVMs in dilute InAsN would be desirable in order to ascertain the origin of the Raman features at 402 and 415 cm^{-1}, since these could arise from N configurations that distort strongly the crystal lattice of the InAs matrix and which could be linked to deviations of Vegard's law in the dilute InAsN alloy.

D. PL and optical absorption

PL and optical measurements have been used in the past to study the dependence on N content of the band gap energy of dilute InAsN.[5,9,11–13,18] The results are usually analyzed in terms of the BAC model, which allows one to calculate the fundamental band gap energy of $InAs_{1-x}N_x$ (i.e., the energy of the E_- subband) as a function of composition[19]

$$E_-(x) = \tfrac{1}{2}[E_N + E_0^{\mathrm{InAs}} - \sqrt{(E_N - E_0^{\mathrm{InAs}})^2 + 4C_{MN}^2 x}], \qquad (1)$$

where E_0^{InAs} is the band gap energy of the InAs matrix, E_N is the energy of the effective N level relative to the valence band maximum, and C_{MN} is the coupling constant for the interaction between the effective N level and the extended conduction states. Unlike the case of Ga(In)AsN alloys, where two conduction subbands E_+ and E_- are detected by optical experiments, only the low-energy conduction band of dilute InAsN has been observed so far. As a consequence, the BAC parameters for InAsN are usually determined with low accuracy. Recently, Zhuang *et al.*[12] performed PL studies on InAsN/InAs samples similar to those studied in this work, and obtained a value of C_{MN}=2.5 eV at 4 K and a value of C_{MN}=2.7 eV at 300 K. Kudrawiec *et al.*[18] reported PR spectra of similar samples with N contents up to ~1% and obtained C_{MN}=2.7 eV at 20 K. Previous studies obtained much lower C_{MN} values (Veal *et al.*[11] found a value of C_{MN} =1.77 eV with PL at 80 K; Shih *et al.*[9] and Kuroda *et al.*[6] performed absorption measurements at 300 K and obtained C_{MN}=1.68 eV and 1.86 eV, respectively, after correcting for the Burstein–Moss effect). Vurgaftman and Meyer[31] give a recommended value of 2.0 eV.

We show in Fig. 5 RT α^2 values, as obtained from optical transmission data from two of the InAsN/InAs samples investigated in this work. Unfortunately, we were not able to detect a distinct absorption edge from all our samples, since

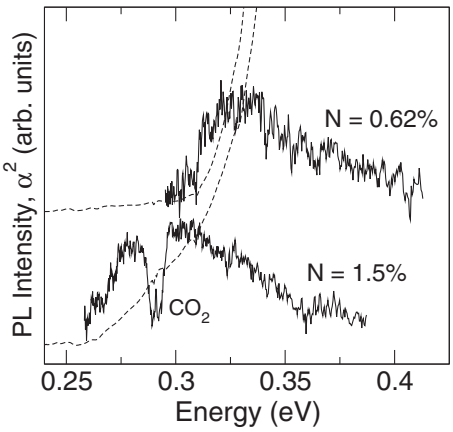

FIG. 5. PL spectra and square of the absorption coefficient vs photon energy for two different InAsN/InAs epilayers.

the transmission spectra of some of them was not flat at the longer wavelengths detected (i.e., for photon energies below the band gap energy). On the other hand, strong absorption from the thick InAs substrate dominates the absorption curves for photon energies only slightly above the absorption edge of InAsN, and as a consequence we were not able to observe the typical linear dependence of α^2 of direct-band gap semiconductors for a sufficiently wide range of photon energies. In spite of this, however, the absorption edge of InAsN shows the expected band gap energy reduction when the N content of the alloy is increased. This can be seen in Fig. 5, where RT PL spectra have been included for comparison.

As discussed in detail elsewhere,[12,13] the RT PL emission from InAsN is quite broad. Absorption bands from atmospheric CO_2 are observed in the PL spectrum of the sample with $N_{XRD}=1.5\%$ (lower curve of Fig. 5). As can be seen in this figure, the onset of absorption in both samples is 20–30 meV below the PL peak energy. This was observed to occur in all the samples that exhibited a clear absorption edge. We plot in Fig. 6 the composition dependence of the band gap energy values as obtained from the PL results, together with the photon energy value corresponding to the onset of optical absorption in InAsN. The dashed lines in the figure are fits carried out by using the BAC model [Eq. (1)]. For the fits, we used a value of $E_N=1.44$ eV (Ref. 31) and left C_{MN} as the only free parameter. We obtain a value of C_{MN}

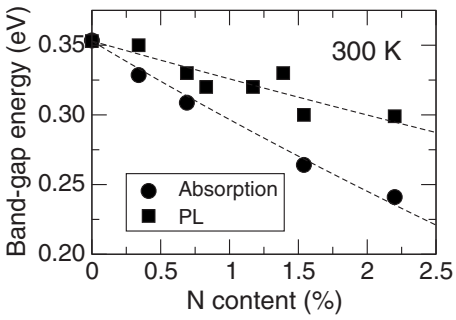

FIG. 6. Band gap energy values of the InAsN epilayers studied in this work as a function of N content. The values are obtained from PL measurements (squares) and optical absorption measurements (circles). The dashed lines are fits to the PL and absorption data with the BAC model, Eq. (1).

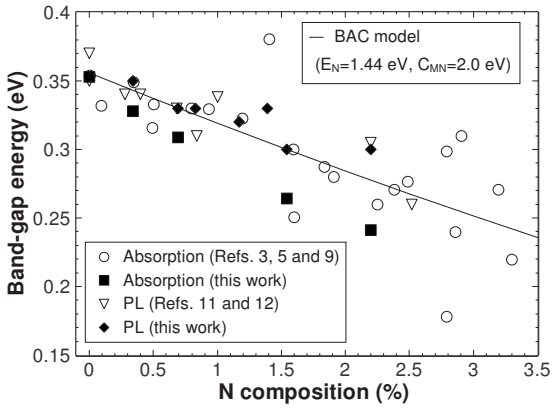

FIG. 7. Band gap energy values at 300 K for the InAsN alloy as obtained from PL and optical absorption measurements published in the literature. Data obtained in this work are also included. The solid line is a fit to all the experimental points by using the BAC model, Eq. (1).

$=1.74$ eV from the fit to the PL data, while $C_{MN}=2.54$ eV is found from the analysis of the absorption data.

Although the values of C_{MN} that we obtain in the present work are in qualitative agreement with the values obtained in previous studies, one cannot overlook the fact that all the band gap values obtained from the optical absorption edge are consistently lower than those obtained from the PL peak energy. Most probably, the onset of absorption in the InAsN samples underestimates the band gap energy owing to disorder-induced band-tailing effects, which are typical of dilute nitrides.[32] Regarding the RT optical emission, the broad PL features observed in these samples are attributed to band-to-band transitions.[12,13] At lower temperatures, emission at longer wavelengths arising from recombination of localized electrons and delocalized holes is also detected.[12,13] Nevertheless, the RT PL signal is usually very weak, and, therefore, high power densities on the samples are employed. Thus, it cannot be ruled out that the RT PL emission is blueshifted by band-gap filling effects originated by strong free-carrier photogeneration.

Figure 7 shows a collection of RT band gap energy values published in the literature for the InAsN alloy, as obtained from PL and absorption measurements.[3,5,9,11,12] The data from the present work has also been included in the figure for completeness. Here, in order to obtain a recommended value for the RT coupling constant C_{MN} for InAsN, we use Eq. (1) to fit the data of Fig. 7. We find that the best C_{MN} value that fits these data is $C_{MN}=2.0\pm0.1$ eV. Thus, our analysis confirms that the best C_{MN} value given by Vurgaftman and Meyer[31] describes well the dependence on N content of the fundamental band gap energy of the InAsN alloy.

IV. CONCLUSIONS

High quality InAsN epilayers with RT PL emission have been grown by MBE on n^+-InAs substrates. A combined analysis of HRXRD and ToF-SIMS measurements suggests that the lattice parameter of InAsN may deviate significantly from Vegard's law as a consequence of nonsubstitutional incorporation of N into the InAsN lattice. We have used Raman scattering to investigate the incorporation of N into the

InAsN alloy. Different N-related LVMs appear in the Raman spectra of our InAsN/InAs samples. FTIR reflectance measurements on InAsN/GaAs epilayers have allowed us to confirm that the main LVM band at 440 cm^{-1} corresponds to substitutional N. The rest of LVM features that appear in the Raman spectra could be related to nonsubstitutional N configurations. These may yield important distortions of the crystal lattice that could account for the observed deviation of Vegard's law. PL and optical transmission measurements have been presented in order to evaluate the composition dependence of the band gap energy in our samples. From the analysis of our optical data as well as data published in the literature, we obtain the RT coupling parameter for the BAC model in InAsN, $C_{NM}=2.0\pm0.1$ eV, in agreement with the value recommended by Vurgaftman and Meyer.[31]

ACKNOWLEDGMENTS

This work supported by the Spanish Ministry of Education and Science (Project No. MAT2007-63617) and by the Engineering and Physical Sciences Research Council, United Kingdom.

[1]For a review on dilute nitride alloys see, M. Henini, *Dilute Nitride Semiconductors* (Elsevier, Amsterdam, 2005).
[2]M. Osinski, Opto-Electron. Rev. **11**, 321 (2003).
[3]H. Naoi, Y. Naoi, and S. Sakai, Solid-State Electron. **41**, 319 (1997).
[4]S. Sakai, T. S. Cheng, T. C. Foxon, T. Sugahura, Y. Naoi, and H. Naoi, J. Cryst. Growth **189–190**, 471 (1998).
[5]M. Kuroda, A. Nishikawa, R. Katayama, and K. Onabe, J. Cryst. Growth **278**, 254 (2005).
[6]M. Kuroda, R. Katayama, S. Nishio, K. Onabe, and Y. Shiraki, Phys. Status Solidi C **0**, 2765 (2003).
[7]M. de la Mare, Q. Zhuang, A. Krier, A. Patanè, and S. Dhar, Appl. Phys. Lett. **95**, 031110 (2009).
[8]J. S. Wang, H. H. Lin, L. W. Song, and G. R. Chen, J. Vac. Sci. Technol. B **19**, 202 (2001).
[9]D. K. Shih, H. H. Lin, L. W. Sung, T. S. Chu, and T.-R. Yang, Jpn. J. Appl. Phys., Part 1 **42**, 375 (2003).
[10]J. Wagner, K. Kohler, P. Ganser, and M. Maier, Appl. Phys. Lett. **87**, 051913 (2005).
[11]T. D. Veal, L. F. J. Piper, P. H. Jefferson, I. Mahboob, C. F. McConville, M. Merrick, T. J. C. Hose, B. N. Murdin, and M. Hopkinson, Appl. Phys. Lett. **87**, 182114 (2005).
[12]Q. Zhuang, M. R. Godenir, A. Krier, K. T. Lai, and S. K. Haywood, J. Appl. Phys. **103**, 063520 (2008).
[13]Q. Zhuang, A. Godenir, and A. Krier, J. Phys. D: Appl. Phys. **41**, 132002 (2008).
[14]D. K. Shih, H. H. Lin, and Y. H. Lin, Electron. Lett. **37**, 1342 (2001).
[15]V. Sallet, L. Largeau, O. Mauguin, L. Travers, and J. C. Harmand, Phys. Status Solidi B **242**, R43 (2005).
[16]W. J. Fan, S. F. Yoon, T. K. Ng, S. Z. Wang, W. K. Loke, R. Liu, and A. Wee, Appl. Phys. Lett. **80**, 4136 (2002).
[17]H. Benaissa, A. Zaoui, and M. Ferhat, J. Appl. Phys. **102**, 113712 (2007).
[18]R. Kudrawiec, J. Misiewicz, Q. Zhuang, A. M. R. Godenir, and A. Krier, Appl. Phys. Lett. **94**, 151902 (2009).
[19]W. Shan, W. Walukiewicz, J. W. Ager III, E. E. Haller, J. F. Geisz, D. J. Friedman, J. M. Olson, and S. R. Kurtz, Phys. Rev. Lett. **82**, 1221 (1999).
[20]J. Ibáñez, E. Alarcón-Lladó, R. Cuscó, L. Artús, and M. Hopkinson, J. Appl. Phys. **102**, 013502 (2007).
[21]R. Carles, N. Saint-Cricq, J. B. Renucci, M. A. Renucci, and A. Zwick, Phys. Rev. B **22**, 4804 (1980).
[22]T. Prokofyeva, T. Sauncy, M. Seon, M. Holtz, Y. Qiu, S. Nikishin, and H. Temkin, Appl. Phys. Lett. **73**, 1409 (1998).
[23]J. Ibáñez, E. Alarcón-Lladó, R. Cuscó, L. Artús, M. Henini, and M. Hopkinson, J. Mater. Sci.: Mater. Electron. **20**, 116 (2009).
[24]Y. B. Li, I. T. Ferguson, R. A. Stradling, and R. Zallen, Semicond. Sci. Technol. **7**, 1149 (1992).
[25]K. Wan and J. F. Young, Phys. Rev. B **41**, 10772 (1990).
[26]J. Ibáñez, R. Cuscó, E. Alarcón-Lladó, L. Artús, A. Patanè, D. Fowler, L. Eaves, K. Uesugi, and I. Suemune, J. Appl. Phys. **103**, 103528 (2008).
[27]R. Cuscó, J. Ibáñez, and L. Artús, Phys. Rev. B **57**, 12197 (1998).
[28]R. Cuscó, J. Ibáñez, E. Alarcón-Lladó, L. Artús, T. Yamaguchi, and Y. Nanishi, Phys. Rev. B **80**, 155204 (2009).
[29]H. C. Alt, A. Y. Egorov, H. Riechert, J. D. Meyer, and B. Wiedemann, Physica B **308–310**, 877 (2001).
[30]A. M. Teweldeberhan and S. Fahy, Phys. Rev. B **77**, 235216 (2008).
[31]I. Vurgaftman and J. R. Meyer, J. Appl. Phys. **94**, 3675 (2003).
[32]U. Tisch, E. Finkman, and J. Salzman, Appl. Phys. Lett. **81**, 463 (2002).